

www.acsabm.org Article

# Development of Human Host Defense Antimicrobial Peptide-Conjugated Biochar Nanocomposites for Combating Broad-Spectrum Superbugs

Ye Gao, Avijit Pramanik, Shamily Patibandla, Kaelin Gates, Glake Hill, Andrew Ignatius, and Paresh Chandra Ray\*



Cite This: ACS Appl. Bio Mater. 2020, 3, 7696-7705



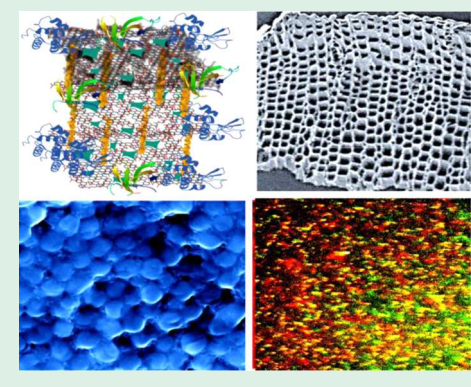
**ACCESS** 

Metrics & More

Article Recommendations

Supporting Information

**ABSTRACT:** Infectious diseases by multidrug-resistant superbugs, which cannot be cured using commercially available antibiotics, are the biggest threat for our society. Due to the lack of discovery of effective antibiotics in the last two decades, there is an urgent need for the design of new broad-spectrum antisuperbug biomaterials. Herein, we report the development of antisuperbug nanocomposites using human host defense antimicrobial peptide-conjugated biochar. To develop an economically viable technology, biochar, a carbon-rich material from naturally abundant resource, has been used. For combating broad-spectrum superbugs, a nanocomposite has been designed by combining biochar with α-defensin human neutrophil peptide-1 (HNP-1), human β-defensin-1 (hBD-1), and human cathelicidin LL-37 antimicrobial peptide. The designed three-dimensional (3D) nanocomposites with pore size between 200 and 400 nm have been used as channels for water passage and captured superbugs. The reported data demonstrated that antimicrobial nanocomposite can be



used for efficient capture and eradication of Gram-negative carbapenem-resistant *Enterobacteriaceae* (*CRE*) *Escherichia coli* (*E. coli*) and *Klebsiella pneumoniae* (*KPN*) superbugs, as well as Gram-positive methicillin-resistant *Staphylococcus aureus* (MRSA) and vancomycin-resistant enterococci (VRE) superbugs. Possible mechanisms for broad-spectrum antisuperbug activities using hydrogel have been discussed.

KEYWORDS: biochar-based nanocomposite, human host defense antimicrobial peptides, Gram-positive bacteria, Gram-negative pathogens, combating broad-spectrum superbugs

#### 1. INTRODUCTION

From 1945, after the availability of antibiotic penicillin in the market, antibiotics became a medical miracle for our society to save millions of lives every year from infectious disease. 1-5 However, in the last few decades, microorganisms developed very smart defense strategies against market available antibiotics.<sup>3-10</sup> As a result, infection diseases due to the drugresistant microorganism cannot be cured using market available antibiotics. 11-20 Since multidrug-resistant organisms are emerging too fast against a new antibiotic even before it reaches the market, new classes of antibiotics have not been discovered since the 1990s. <sup>21–30</sup> In the last few years, we and other groups have demonstrated that gold, silver, carbon, graphene oxide, MoS2, WS2, metal oxide, and other nanomaterial-based different approaches, including antimicrobial peptide-attached nanoarchitecture, can be highly promising antimicrobial materials to combat superbugs.<sup>6,7,11,18–33</sup> Most of the reported nanomaterial-based approaches show that single-type antimicrobial peptide-attached nanocomposites can be used for combating either Gram-positive or Gram-negative bacteria. 6,7,11,18-33 In this manuscript, we have reported the

development of three different types human host defense antimicrobial peptide-attached naturally abundant biocharbased novel broad-spectrum antimicrobial nanocomposites.

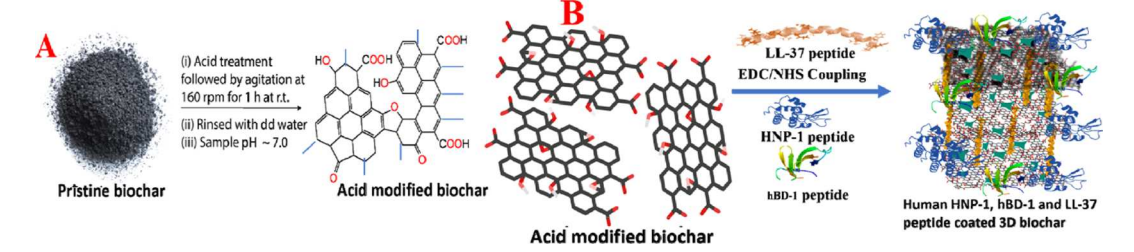
Experimentally measured data show that antimicrobial nanocomposite can be used for 100% of capture and total eradication of Gram-negative carbapenem-resistant *Enterobacteriaceae* (*CRE*) *Escherichia coli* (*E. coli*) and *Klebsiella pneumoniae* (*KPN*) superbugs, as well as for Gram-positive methicillin-resistant *Staphylococcus aureus* (MRSA) vancomycin-resistant enterococci (VRE) superbugs. A 100% capturing and killing efficiency was obtained by attaching biochar with  $\alpha$ -defensin human neutrophil peptide-1 (HNP-1), human  $\beta$ -defensin-1 (hBD-1), and human cathelicidin LL-37 antimicrobial peptide simultaneously.

Received: July 16, 2020 Accepted: October 21, 2020 Published: October 30, 2020





Scheme 1. Schematic Representation Showing the Synthetic Pathway Used to Develop Human Antimicrobial  $\alpha$ -Defensin HNP-1,  $\beta$ -Defensin hBD-1, and Cathelicidin LL-37 Peptide-Attached Biochar Nanocomposites<sup> $\alpha$ </sup>



<sup>a</sup>(A) Development of acid-modified biochar from pristine biochar. (B) Development of 3D biochar nanocomposite from acid-modified biochar.

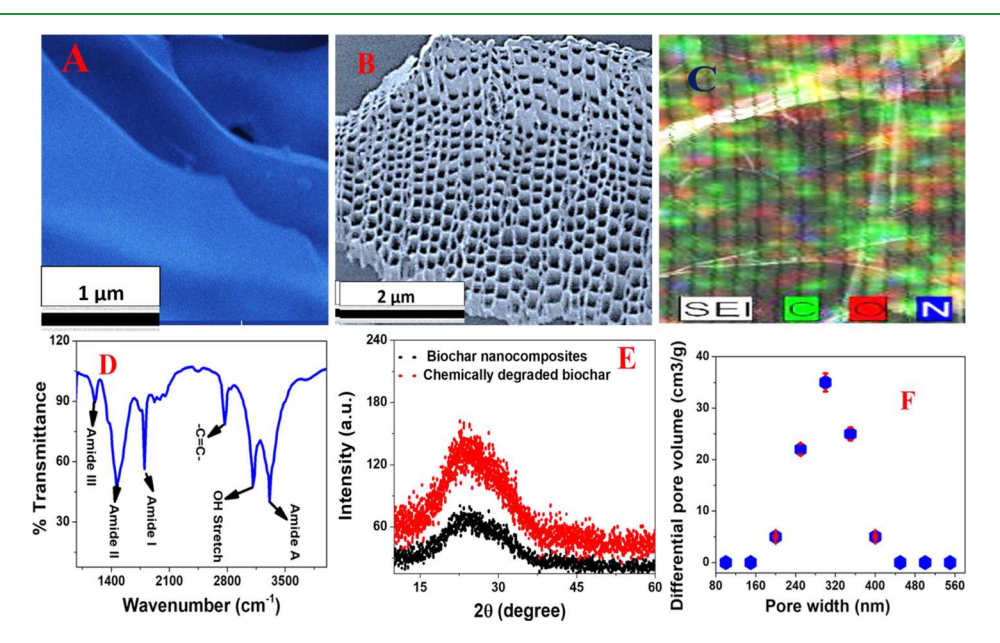


Figure 1. (A) SEM image showing the morphology of chemically degraded biochar through acidic oxidation. (B) SEM image showing the morphology of antimicrobial HNP-1, hBD-1, and LL-37 peptide-attached biochar nanocomposites. (C) EDX mapping showing the presence of C, N, and O on the HNP-1, hBD-1, and LL-37 peptide-attached biochar nanocomposites. The inserted high-resolution image indicates that peptides are attached with biochar. (D) FTIR spectra of human antimicrobial α-defensin HNP-1, β-defensin hBD-1, and cathelicidin LL-37 peptide-attached biochar nanocomposites, which shows the presence of -C=C stretch, -OH stretch, amide-A, amide-II, and amide-III vibrational bands. (E) XRD spectra of chemically degraded biochar and biochar nanocomposites, which show the presence of the (002) reflection of graphite. (F) Pore size distributions from antimicrobial HNP-1, hBD-1, and LL-37 peptide-attached biochar nanocomposites, which shows pore size ranging from 200 to 400 nm and highest density at around 310 nm.

Biochar, a carbon-rich, sustainable, and naturally abundant resource-based green material, has been used to design nanocomposites for environmental applications.  $^{34-39}$  Due to the possibility of large-scale production at low cost, biocharbased nanocomposites will have a great potential for the development of the economically viable medical technology.  $^{34-39}$  Like graphene oxide (GO), acid-modified biochar contains abundant oxygen-containing surface functional groups such as C=O, COOH, and -OH, which have been used to anchor with  $\alpha$ -defensin HNP-1,  $\beta$ -defensin hBD-1, and LL-37 antimicrobial peptide via a covalent bond.  $^{17-22}$  In our design, biochar-based three-dimensional (3D) nanocomposites with pore size between 200 and 400 nm have been used as channels for water passage and to capture drug-resistant pathogens.

Human host defense antimicrobial peptides are very important components of our immunity system to protect from bacterial infections. <sup>40–48</sup> Defensin antimicrobial peptides are cysteine-rich, cationic peptides, which can be classified into two subtypes:  $\alpha$ - and  $\beta$ -defensins. <sup>40–48</sup>  $\alpha$ -Defensin human neutrophil  $\alpha$ -defensin-1 is produced by neutrophils, and it has

the ability to kill pathogens via inhibition of cell-wall synthesis by binding to lipid II and also by membrane lysis.  $^{42,43}$   $\beta$ -Defensin-1 peptides are produced in the epithelium and it has the ability to kill pathogens via blocking of epithelial invasion as well as via membrane lysis. 44,45 On the other hand, cathelicidin family antimicrobial peptides are produced in the epithelium and in neutrophils. 46,47 Cathelicidin LL-37 antimicrobial peptide has the ability to kill pathogens via pore formation in bacterial membranes. 46-48 In our design, we have used α-defensin (ACYCRIPACIAGERRYGTCIYQGRL-WAFCC), β-defensin (GNFLTGLGHRSDHYCVSSGGQ-CLYSACPIFTKIQGTCYRGKAKCCK), and cathelicidin LL-37 (LLGDFFRKSKEKRIVQRIKDFLRNLVPRTES) antimicrobial peptide-attached nanocomposite. Human antimicrobial agents such as  $\alpha$ -defensin HNP-1,  $\beta$ -defensin hBD-1, and LL-37 contain amine groups that have been exploited for functionalization by amide bond formation with carboxyl groups of biochar, as shown in Scheme 1. Reported data show that nanocomposite can exhibit 100% killing efficiency for Gram-negative and Gram-positive superbugs; on the other hand, the killing efficiency is >50% when a mixture of HNP-1, HBD-1, and LL-37 peptides is used without nanocomposites.

#### 2. RESULTS AND DISCUSSION

2.1. Development and Characterization of Chemically Degraded Biochar. Initially, we have performed chemical oxidation of the biochar surface to increase the oxygen-containing functional groups such as -OH, -COOH, etc., as shown in Scheme 1A. For this purpose, biochar powder purchased from Thermo Fisher Scientific (catalog number NC1713201) was used for chemical oxidation without further purification, followed by an acid treatment using a modified literature procedure. <sup>31–36</sup> For chemical oxidation of the biochar surface, biochar powder was immersed in sulfuric acid and nitric acid.<sup>23</sup> Experimental details are given in the Supporting Information. After that, chemical oxidation was conducted by agitation of the mixture at 160 rpm for 1 h at room temperature.<sup>23</sup> After that, to remove the residual acid, the mixture was washed with water several times to reach an approximate pH of 7.0. In the next step, drying of the chemical oxidation was conducted through lyophilization. Finally, we have used high-resolution scanning electron microscopy (SEM) to determine the morphology of chemically degraded biochar, as shown in Figure 1A, which shows a twodimensional (2D) structure. Figure S1B in the Supporting Information shows a high-resolution transmission electron microscopy (HRTEM) image of chemically degraded biochar, which also indicates the 2D structure. The HRTEM image data indicate the stripe distance of ~0.23 nm, which is due to the graphite structure. 34,35 Figure 1E shows the powder X-ray diffraction (XRD) spectrum from chemically degraded biochar, where we have observed the peak at 26.5°, which can be assigned to be the (002) refection of graphite.<sup>34,35</sup> We have also measured the  $\zeta$ -potential ( $\zeta$ ) using a ZetaSizer Nano ZS, Malvern Instruments.  $\zeta$ -Potential measurement indicates that after functionalization, the  $\zeta$ -potential for biochar increases from  $-16 \pm 1$  to  $-34 \pm 1$  mV, which indicates the functionalization of negative charge for oxygen-containing functional groups on surface. The energy-dispersive X-ray (EDX) data reported in Figure S1 in the Supporting Information show the presence of C and O on the chemically oxidized biochar. The Fourier transform infrared (FTIR) spectrum in Figure S2 in the Supporting Information shows -C=O and -OH stretching bands, which indicate carboxylic acidic groups attached on biochar.

2.2. Development and Characterization of HNP-1, hBD-1, and LL-37 Peptide-Attached Biochar Nanocomposites. For the development of broad-spectrum antimicrobial nanocomposites, we have attached chemically degraded biochar with HNP-1, hBD-1, and LL-37 antimicrobial peptide. Since acid-modified biochar contains abundant oxygen-containing surface functional COOH groups and all human host defense antimicrobial agents contain amine groups, we have used carbodiimide coupling chemistry for the development of nanocomposites. As shown in Scheme 1B, for this purpose, initially, carboxyl groups from biochar were activated using 1-ethyl-3(3-(dimethylamino)-propyl)carbodiimide·HCl (EDC) and N-hydroxysuccinimide (NHS) coupling agents for 30 min. 18,19,33 After that, different antimicrobial agents, such as HNP-1, hBD-1, and LL-37, were added at different weight ratios under stirring. In the next step, we have continued the process for 24 h. After that, we

have performed centrifugation at 10 000 rpm for 30 min, followed by decantation.

Finally, the nanocomposites were resuspended in phosphatebuffered saline (PBS) and stored in a refrigerator for further use. After that, SEM and HRTEM were used to determine the morphology of nanocomposites, as shown in Figures 1B and S1C in the Supporting Information. The SEM image clearly shows three-dimensional (3D) porous architecture. The TEM image also indicates the 3D structure. The inserted HRTEM image in Figure S1C indicates the graphite structure, with a stripe distance of  $\sim 0.25$  nm. <sup>34,35</sup> Figure 1E shows the powder X-ray diffraction (XRD) spectrum from antimicrobial peptideattached nanocomposite, where the main peak at 26.5° is assigned to the (002) refection for graphite. 34,35 As shown in Figure 1F, the Barrett-Joyner-Halenda (BJH) analysis data of antimicrobial peptide-attached nanocomposite indicate that the pore size ranges from 200 to 400 nm. The energydispersive X-ray (EDX) data as reported in Figure 1C show the presence of C, O, and N. The EDX data from chemically degraded biochar, as shown in Figure S1A, indicate no nitrogen content on chemically oxidized biochar. EDX measurement after functionalization with  $\alpha$ -defensin human neutrophil peptide-1 (HNP-1), human  $\beta$ -defensin-1 (hBD-1), and human cathelicidin LL-37 antimicrobial peptide indicates around 10 atomic % nitrogen, which indicates the successful immobilization of antimicrobial peptides by EDC/NHS coupling chemistry. Similarly, the attachment of the antimicrobial peptide on the biochar surface was also confirmed by X-ray photoelectron spectroscopy (XPS), as shown in Figure S3 and Table S1 in the Supporting Information. We have not observed any nitrogen peak ~400 eV from biochar; on the other hand, we have observed ca. 8-10 atomic % nitrogen from the nanocomposite. Deconvolution of the nitrogen peaks indicates the presence of NHC=O and -C-NH<sub>2</sub> peaks. The surface chemistry of the nanocomposites was also studied using Fourier transform infrared (FTIR) spectroscopy. As shown in Figure 1D, the FTIR spectra from the antimicrobial peptide-attached biochar-based nanocomposite show the presence of -amide-A, -OH, -amide-I, -C=C-, amide-II, and amide-III. The experimentally observed different amide bands in the XPS data and FTIR spectra indicate that biochar is attached with different peptides in nanocomposites.

To determine the amounts of peptides attached with biochar, we have used dye-labeled peptides. For this purpose, we have used Alexa Fluor 405 dye-labeled human neutrophil peptide-1 (HNP-1) whose fluorescence maximum is at 421 nm. Similarly, we have a Cy3 dye-labeled human  $\beta$ -defensin-1 (hBD-1) peptide, whose fluorescence maximum is at 568 nm. We have also used a Cy5 dye-labeled human cathelicidin LL-37 antimicrobial peptide, whose fluorescence maximum is at 666 nm. After finishing the coupling between peptides and biochar, we have removed the excess unreacted dye-labeled peptides by washing with deionized water. By measuring the fluorescence from supernatant, we were able to measure the amount of excess peptides that were not coupled. We have also measured the fluorescence from peptide-attached nanocomposites, and from both measurement data, we have estimated ~85% coupling efficiency for α-defensin human neutrophil peptide-1 (HNP-1), ~81% coupling efficiency for human  $\beta$ -defensin-1 (hBD-1), and ~87% coupling efficiency for human cathelicidin LL-37 antimicrobial peptide.

**ACS Applied Bio Materials** 

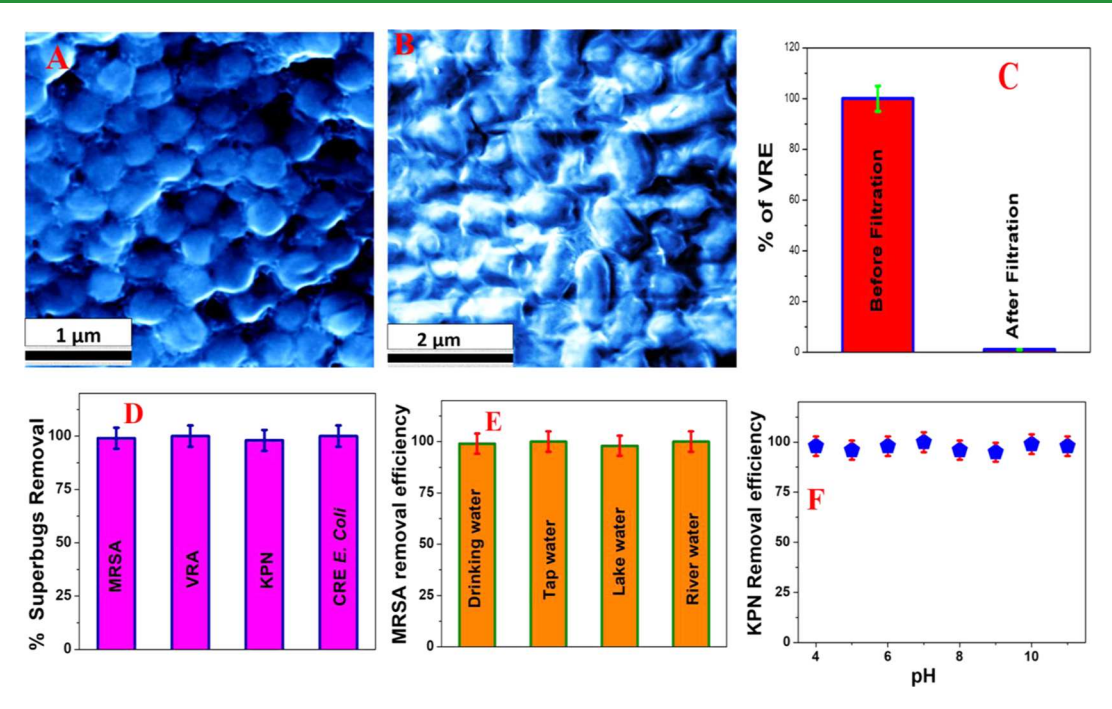


Figure 2. (A) Top-view SEM image after filtration of MRSA-contaminated water using  $\alpha$ -defensin human neutrophil peptide-1, human  $\beta$ -defensin-1, and human cathelicidin LL-37 antimicrobial peptide-attached nanocomposites. The image shows that MRSA superbugs are captured by nanocomposites. (B) Top-view SEM image after filtration of CRE *E. coli*-contaminated water using antimicrobial conjugate nanocomposites. The image shows that CRE *E. coli* superbugs are captured by nanocomposites. (C) Plot showing the percentage of VRE superbugs removed from water using  $\alpha$ -defensin human neutrophil peptide-1, human  $\beta$ -defensin-1, and human cathelicidin LL-37 antimicrobial peptide-attached nanocomposite, when the VRE concentration was 6.4 × 10<sup>5</sup> CFU/mL. (D) Superbug removal efficiency for the mixture of MRSA, CRE *E. coli*, KPN, and VRE in water (1.6 × 10<sup>5</sup> CFU/mL concentration for each superbug) using HNP-1, hBD-1, and human cathelicidin LL-37 antimicrobial peptide-attached nanocomposite. (E) Plot showing how the source of water influences the MRSA superbug removal efficiency using HNP-1, hBD-1, and human cathelicidin LL-37 antimicrobial peptide-attached nanocomposite, when MRSA concentration was 6.4 × 10<sup>5</sup> CFU/mL. (F) Plot showing how pH of water influences the removal efficiency for *KPN* superbugs from drinking water using  $\alpha$  antimicrobial peptide-attached nanocomposite., when KPN concentration was 6.4 × 10<sup>5</sup> CFU/mL.

We have also determined the specific surface area for antimicrobial peptide-attached nanocomposite using  $N_2$  adsorption/desorption data and a Tristar II 3020 surface area analyzer.  $^{18,19,33}$  From the  $N_2$  adsorption/desorption data, we found out that the specific surface area for our antimicrobial peptide-attached nanocomposite is 386  $\rm m^2/g$ , with a pore volume of 0.872 cm³/g. We have also measured the water flux for antimicrobial peptide-attached nanocomposite, and we have estimated the water flux for nanocomposites to be 308.6 L/(m² h bar). We have also measured the  $\zeta$ -potential, which indicates that after functionalization with antimicrobial peptides, the  $\zeta$ -potential for biochar decreases from to  $-34\pm1$  to  $-4.5\pm1$  mV, which indicates the functionalization of positive-charge antimicrobial peptides on biochar surface.

2.3. Use of Antimicrobial HNP-1, hBD-1, and LL-37 Peptide-Conjugated Biochar-Based Nanocomposites for Separation of Superbugs from Water Sample. Next, we have tested whether HNP-1, hBD-1, and LL-37 peptide-attached biochar-based nanocomposite can be used for capturing and removing superbugs from the environmental water sample. The experimental details for the superbugs sample preparation are reported in the Supporting Information. For this purpose, first, we have infected the drinking water sample with Gram-negative CRE E. coli, and KPN superbugs, as well as Gram-positive MRSA and VRE superbugs, selectively and simultaneously.

For the selective captured experiment, we have used a  $6.4 \times 10^5$  CFU/mL concentration of each MRSA, CRE *E. coli*, KPN,

and VRE superbug. For the mixture of MRSA, CRE E. coli, KPN, and VRE superbugs experiment, we have used a 1.6  $\times$ 10<sup>5</sup> CFU/mL concentration for each superbug. In the next step, we have performed filtration of superbug-infected water sample using  $\alpha$ -defensin human neutrophil peptide-1, human β-defensin-1, and human cathelicidin LL-37-attached biocharbased nanocomposites. After separation of MRSA, CRE E. coli, KPN, and VRE superbugs via filtration, we have used the colony plating technique on lysogeny broth (LB) agar<sup>18,19,33</sup>as well as reverse transcription polymerase chain reaction (RT-PCR) techniques <sup>18,19,33</sup> for finding the removal efficiency of different drug-resistant bacteria using  $\alpha$ -defensin human neutrophil peptide-1, human  $\beta$ -defensin-1, and human cathelicidin LL-37-attached biochar-based nanocomposites. Experimental details are discussed in the Supporting Information. As reported in Figure 2C,D, the percentage of superbugs removal data clearly shows that 100% of VRE, MRSA, CRE E. coli, and KPN superbugs can be captured selectively or simultaneously, using  $\alpha$ -defensin human neutrophil peptide-1, human  $\beta$ -defensin-1, and human cathelicidin LL-37-attached biochar-based nanocomposites. The experimentally observed very high superbug capturing efficiency for VRE, MRSA, CRE E. coli, and KPN using the antimicrobial peptide-attached biochar-based nanocomposite is due to the fact that the size of VRE, MRSA, CRE E. coli, and KPN superbugs is between 500 and 2000 nm, which is much higher than the pore size of antimicrobial peptide-attached biochar-based nanocomposite (200-400 nm).

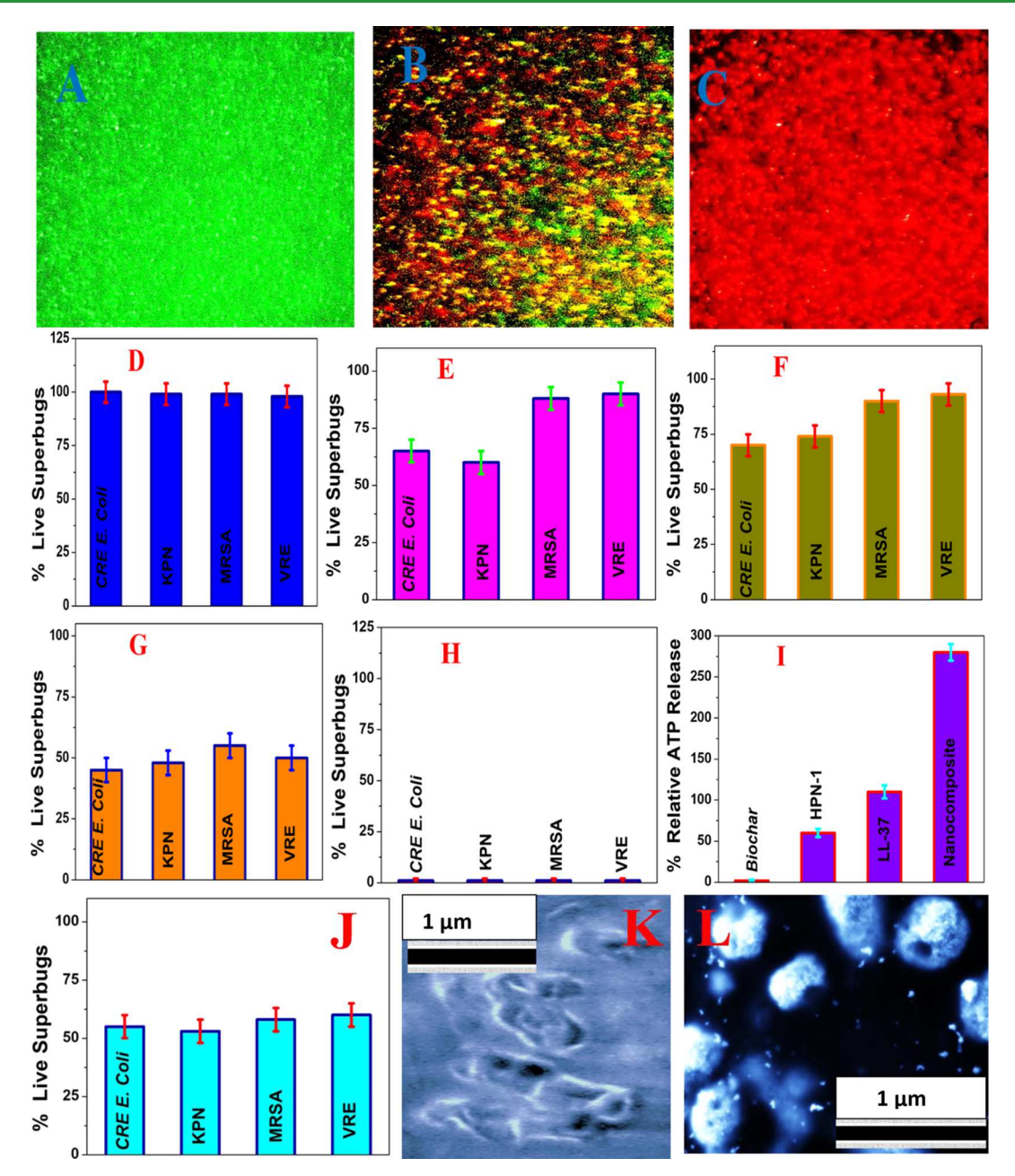


Figure 3. (A) Viability of CRE E. coli after exposure with biochar. Live/Dead kit was used to stain bacteria. Green fluorescence indicates live bacteria. (B) Viability of CRE E. coli after exposure to human cathelicidin LL-37 antimicrobial peptide (18 µg/mL)-attached biochar. Live/Dead kit was used to stain bacteria. Green fluorescence indicates live bacteria, and red fluorescence indicates dead bacteria. The observed yellow fluorescence is due to the overlap of green and red fluorescence. (C) Viability of CRE E. coli after exposure to  $\alpha$ -defensin human neutrophil peptide-1 (6 μg/mL), human β-defensin-1 (6 μg/mL), and human cathelicidin LL-37 (6 μg/mL)-attached biochar-based nanocomposite. Live/ Dead kit was used to stain bacteria. Red fluorescence indicates dead bacteria. (D) Comparison of the superbug-killing efficiency for VRE, MRSA, CRE E. coli, and KPN drug-resistant bacteria, when these superbugs were exposed to only biochar. (E) Comparison of the superbug-killing efficiency for VRE, MRSA, CRE E. coli, and KPN drug-resistant bacteria, when these superbugs were exposed to  $\alpha$ -defensin human neutrophil peptide-1 (18 µg/mL)-attached biochar. (F) Comparison of the superbug-killing efficiency for VRE, MRSA, CRE E. coli, and KPN drug-resistant bacteria, when these superbugs were exposed to human  $\beta$ -defensin-1 (18  $\mu$ g/mL)-attached biochar. (G) Comparison of the superbug-killing efficiency for VRE, MRSA, CRE E. coli, and KPN drug-resistant bacteria, when these superbugs were exposed to human cathelicidin LL-37 peptide-1 (18 μg/mL)-attached biochar. (H) Comparison of the superbug-killing efficiency for VRE, MRSA, CRE E. coli, and KPN drug-resistant bacteria, when these superbugs were exposed to  $\alpha$ -defensin human neutrophil peptide-1 (6  $\mu$ g/mL), human  $\beta$ -defensin-1 (6  $\mu$ g/mL), and human cathelicidin LL-37 (6 µg/mL)-attached biochar-based nanocomposite. (I) Plot showing relative cellular ATP leakage percentage for CRE E. coli when bacteria were treated with biochar,  $\alpha$ -defensin human neutrophil peptide-1 (18  $\mu$ g/mL), human cathelicidin LL-37 peptide-1 (18  $\mu$ g/mL),  $\alpha$ defensin human neutrophil peptide-1 (6  $\mu$ g/mL), human  $\beta$ -defensin-1 (6  $\mu$ g/mL), and human cathelicidin LL-37 (6  $\mu$ g/mL)-attached biocharbased nanocomposite. (J) Comparison of the superbug-killing efficiencies for VRE, MRSA, CRE E. coli, and KPN drug-resistant bacteria, when these superbugs were exposed to  $\alpha$ -defensin human neutrophil peptide-1 (6  $\mu$ g/mL), human  $\beta$ -defensin-1 (6  $\mu$ g/mL), and human cathelicidin LL-37 (6 μg/mL) simultaneously without biochar. (K) SEM image clearly showing membrane damage on KPN bacteria surface when they are exposed to biochar-based nanocomposite. (L) SEM image clearly showing membrane damage on MRSA bacteria surface when they are exposed to biocharbased nanocomposite.

Since the size of water is much less than the size of the antimicrobial peptide-attached biochar-based nanocomposite, water can pass through it very easily. On the other hand, due to the much bigger size of VRE, MRSA, CRE E. coli, and KPN superbugs, these drug-resistant bacteria will not be able to pass through the  $\alpha$ -defensin human neutrophil peptide-1, human  $\beta$ -defensin-1, and human cathelicidin LL-37-attached biocharbased nanocomposite, and as a result, they will be captured. To characterize captured drug-resistant bacteria during filtration by antimicrobial peptide-attached biochar-based nanocomposite, we have performed a high-resolution SEM experiment. The SEM images in Figure 2A,B clearly show that MRSA and CRE E. coli superbugs are captured on the surface of biocharbased nanocomposites.

Since the pH of water from different sources can be different, before testing whether  $\alpha$ -defensin human neutrophil peptide-1, human  $\beta$ -defensin-1, and human cathelicidin LL-37attached biochar-based nanocomposite can be used for capturing and removing superbugs from the environmental water sample, we have done experimental determination on how the pH of the water can influence the removal efficiency for superbugs. Figure 2F reports the experimental data, which indicate that the removal efficiency for KPN superbugs is almost independent of pH of water within the range of acidic pH 4 to alkaline pH 11. The experimentally observed pHindependent KPN superbugs capture efficiency, as reported in Figure 2F, is due to the fact that the KPN superbugs are larger than 1000 nm and are captured by antibacterial peptideattached biochar-based nanocomposite whose pore size is below 400 nm. It is now well documented that pH change can only change the protonation or deprotonation character for the functional groups attached with the biochar-based nanocomposite. Since the change of pH does not affect the pore size of antibacterial peptide-attached biochar-based nanocomposite abruptly, we have observed no significant change for KPN superbugs capturing efficiency as we vary the pH of water from 4 to 11. Figure 2E shows the variation of MRSA superbug removal efficiency for environmental water sample collected from tap water, lake water, and Mississippi River water, and MRSA superbugs were infected at  $1.6 \times 10^5$  CFU/ mL concentration. The experimental data reported in Figure 2E clearly show that the  $\alpha$ -defensin human neutrophil peptide-1, human  $\beta$ -defensin-1, and human cathelicidin LL-37-attached biochar-based nanocomposite can be used for capturing and removing 100% of MRSA superbugs from environmental water sample.

2.4. Use of Antimicrobial Peptide-Conjugated Biochar-Based Nanocomposites for Eradication of Gram-Negative CRE E. coli and KPN Superbugs, as well as Gram-Positive MRSA and VRE Superbugs Captured by **Nanocomposites.** Here, we will show that *VRE*, MRSA, CRE E. coli, and KPN superbugs can be transmitted through contaminated water. For real-life applications, it is extremely important that the antimicrobial peptide-attached biochar-based nanocomposite has the capability to kill superbugs after capturing. 2-10 To determine the amounts of superbugs killed after capturing by antibacterial peptideattached biochar-based nanocomposite, we have performed colony plating and Live/Dead BacLight molecular probes' assays. 18,19,23 Experimental details are reported in the Supporting Information. Figure 3A-C shows the microscopic images of Live/Dead molecular probes' assays for the viability of carbapenem-resistant Enterobacteriaceae (CRE) E. coli after exposure with biochar, human cathelicidin LL-37, and antimicrobial peptide (18  $\mu$ g/mL)-attached biochar and  $\alpha$ defensin human neutrophil peptide-1 (6  $\mu$ g/mL), human  $\beta$ defensin-1 (6  $\mu$ g/mL), and human cathelicidin LL-37 (6  $\mu$ g/ mL)-attached biochar-based nanocomposite. Live/Dead assay is a two-color fluorescence assay, which utilizes mixtures of our SYTO 9 green-fluorescent nucleic acid stain and propidium iodide red-fluorescent nucleic acid stain. 18,19,23 Since SYTO 9 green-fluorescent nucleic acid stain binds with the live bacteria, in the microscopy image, the green-color image indicates live bacteria. 18,19,23 As shown in Figure 3A, 100% of CRE E. coli are alive after exposure with biochar. On the other hand, propidium iodide red-fluorescent nucleic acid stain only binds with dead bacteria, and in the microscopy image, the red-color image indicates dead bacteria. 18,19,23 As shown in Figure 3C, 100% of CRE E. coli are killed after exposure with  $\alpha$ -defensin human neutrophil peptide-1 (6  $\mu$ g/mL), human  $\beta$ defensin-1 (6  $\mu$ g/mL), and human cathelicidin LL-37 (6  $\mu$ g/ mL)-attached biochar-based nanocomposite. Similarly, when some bacteria are dead and some are alive, it will be a mixture of red and green. When red and green combine, the result is yellow, and we have also observed yellow fluorescence due to the overlap of fluorescence from live and dead bacteria. As reported in Figure 3B, we have observed a mixture of red, green, and yellow fluorescent images when CRE E. coli is exposed to human cathelicidin LL-37 antimicrobial peptide (18 µg/mL)-attached biochar, which indicates that CRE E. coli is partially killed.

To understand why the human cathelicidin LL-37 antimicrobial peptide (18 µg/mL)-attached biochar kills CRE E. coli partially and  $\alpha$ -defensin human neutrophil peptide-1 (6  $\mu g/mL$ ), human  $\beta$ -defensin-1 (6  $\mu g/mL$ ), and human cathelicidin LL-37 (6 µg/mL)-attached biochar-based nanocomposite kill CRE E. coli totally, we have explored the superbug-killing mechanism. For this purpose, we have also developed  $\alpha$ -defensin human neutrophil peptide-1 (18  $\mu$ g/ mL), human  $\beta$ -defensin-1 (18  $\mu$ g/mL), and human cathelicidin LL-37 (18  $\mu$ g/mL)-attached biochar. After that, we have performed superbug-killing activity for each biochar using Gram-negative carbapenem-resistant CRE E. coli and KPN superbugs, as well as Gram-positive MRSA and VRE superbugs, separately. As shown in Figure 2D, the superbugkilling efficiency is about 0% when only biochar was used. On the other hand, as shown in Figure 3E,  $\alpha$ -defensin human neutrophil peptide-1 (18 µg/mL)-attached biochar can kill around 30% for Gram-negative CRE E. coli and KPN superbugs and around 15% for Gram-positive MRSA and VRE superbugs. The above data clearly indicate that HPN-1 antimicrobial peptide is necessary to kill superbugs that are captured by biochar-based nanocomposites.

Human neutrophil peptide-1 (HNP-1) is known to kill bacteria through membrane pore formation, which results in leakage of intracellular contents and cell lysis. 42-45 It also has the ability to bind to cell-wall precursor lipid II, which helps the inhibition of cell-wall synthesis. To understand the lower killing efficiency of HPN-1 antimicrobial peptide for Gram-positive superbugs than Gram-negative superbugs, as reported in Figure 3E, we have determined the minimum inhibitory concentrations (MICs) for HPN-1 antimicrobial peptide-attached biochar against *CRE E. coli* and MRSA, using the National Committee for Clinical Laboratory Standards (NCCLS), as we have reported before. 18,19,23,36 From the experimental data, we have determined the MICs of HPN-1

antimicrobial peptide, which is 52  $\mu$ M for *CRE E. coli* and 95  $\mu$ M for *VRE*. Since we have used only 18% antimicrobial peptide-attached biochar, we have observed around 30% killing efficiency for Gram-negative *CRE E. coli* and 15% killing efficiency for Gram-positive VRE superbug.

Similarly, human  $\beta$ -defensin-1 has the ability to kill pathogens via blocking of epithelial invasion as well as via membrane lysis. 42–44 As shown in Figure 3F, human  $\beta$ -defensin-1-attached biochar can kill around 25% for Gramnegative *CRE E. coli* and *KPN* superbugs and around 10% for Gram-positive MRSA and VRE superbugs. We have determined the MICs of human  $\beta$ -defensin-1 antimicrobial peptide, which is 60  $\mu$ M for *CRE E. coli* and 112  $\mu$ M for *VRE*. Since we have used only 18% antimicrobial peptide-attached biochar, we have observed around 25% killing efficiency for Gram-negative *CRE E. coli* and 10% killing efficiency for Gram-positive VRE superbug.

On the other hand, human cathelicidin family LL-37 antimicrobial peptide has the ability to kill pathogens via pore formation in bacterial membranes, via interfering DNA transcription. As shown in Figure 3G, human cathelicidin family LL-37 antimicrobial peptide-attached biochar can kill around 55% Gram-negative CRE E. coli and KPN superbugs and around 45% Gram-positive MRSA and VRE superbugs. We have determined the MICs of human cathelicidin family LL-37 antimicrobial peptide, which is 34  $\mu$ M for CRE E. coli and 41  $\mu$ M for VRE. Since we have used only 18% antimicrobial peptide-attached biochar, we have observed around 55% killing efficiency for Gram-negative CRE E. coli and 45% killing efficiency for Gram-positive VRE superbug.

As shown in Figure 3H, we have observed 100% killing efficiency for  $\alpha$ -defensin human neutrophil peptide-1 (6  $\mu$ g/mL), human  $\beta$ -defensin-1 (6  $\mu$ g/mL), and human cathelicidin LL-37 (6  $\mu$ g/mL)-attached biochar-based nanocomposite. Although we have used the same amount of antimicrobial peptide (total 18  $\mu$ g/mL), the nanocomposite can kill 100% Gram-negative *CRE E. coli* and *KPN* superbugs as well as Gram-positive MRSA and VRE superbugs. The above data clearly indicate that our nanocomposites can be used for combating broad-spectrum superbugs.

The observed 100% killing efficiency of superbugs using three different peptide-attached biochar-based nanocomposites can be due to the fact that when superbugs are captured by nanocomposites, it causes high membrane stress. It becomes a very good condition for all three  $\alpha$ -defensin human neutrophil peptide-1, human  $\beta$ -defensin-1, and human cathelicidin LL-37 peptides to bind to the surface of bacteria by electrostatic interaction. In this situation, three different antimicrobial peptides will kill 100% of bacteria via several pathways synergistically. HNP-1 will kill bacteria through membrane pore formation, which results in leakage of intracellular contents and cell lysis. 40-48 On the other hand, human  $\beta$ defensin-1 will kill pathogens via blocking of epithelial invasion as well as via membrane lysis. 40–48 Similarly, human cathelicidin family LL-37 antimicrobial peptide will kill pathogens via pore formation in bacterial membranes as well as via interfering DNA transcription. 40-48 Since in this case, different mechanisms of action have been used simultaneously, nanocomposites have the ability to kill 100% Gram-positive and Gram-negative superbugs via synergistic killing effects. To understand whether capturing of superbugs by nanocomposites, which causes high membrane stress, is an important factor for killing Gram-positive and Gram-negative superbugs

simultaneously, we have also performed experiment with the mixture of  $\alpha$ -defensin human neutrophil peptide-1 (6  $\mu$ g/mL), human  $\beta$ -defensin-1 (6  $\mu$ g/mL), and human cathelicidin LL-37  $(6 \mu g/mL)$  without biochar. As reported in Figure 3J, we found that the killing efficiency is >50% for Gram-positive and Gram-negative superbugs. Similarly, we have also performed experiment with biochar flakes (ca. 20-40 nm size; TEM image is shown in Figure S4 in the Supporting Information)attached peptide. As reported in Table S2 in the Supporting Information, the killing efficiency was ~55%. To compare the killing efficiencies with gold nanoparticle-attached peptides, we have performed experiment with spherical gold nanoparticles (~25 nm size; TEM image is shown in Figure S5 in the Supporting Information) attached with  $\alpha$ -defensin human neutrophil peptide-1 (6  $\mu$ g/mL), human  $\beta$ -defensin-1 (6  $\mu$ g/ mL), and human cathelicidin LL-37 (6  $\mu$ g/mL). As reported in Table S2 in the Supporting Information, the killing efficiency was ~62%. All of the reported experimental data clearly indicate that capturing of superbugs by nanocomposites and imposing high membrane stress on bacteria surface are very important for all three peptides to bind to the surface of bacteria and to obtain 100% killing efficiency. When one end of the peptide is conjugated with biochar surface, the cationic side chains of the peptide will interact with negatively charged phospholipids of the bacterial membrane. As a result, disruption of the membrane will take place. The SEM image in Figure 3K,L shows membrane damage on KPN and MRSA bacteria surface, when they are exposed to biochar-based nanocomposites. The above process will cause increased permeability, which will lead to leakage of cell organelles.

To understand better, we have performed bacterial ATP leakage experiment using molecular probes ATP determination kit, as we have reported before.  $^{18,19,23}$  The experimental details are reported in the Supporting Information. Since poly-(ethylene glycol) (PEG)-coated gold nanoparticle is known to be nontoxic for superbugs, we have used PEG-coated gold nanoparticles as reference.  $^{18,19,36}$  Figure 3I shows the ATP leakage experimental data, which indicate that  $\alpha$ -defensin human neutrophil peptide-1, human  $\beta$ -defensin-1, and human cathelicidin LL-37-attached biochar-based nanocomposites can lead to high leakage of cellular ATP for CRE *E. coli*. The reported data indicate that  $\alpha$ -defensin human neutrophil peptide-1 and human cathelicidin LL-37 also promote leakage of cellular ATP, but the amount is much lower than that of the nanocomposite.

In this study, it is clear that integrating antimicrobial peptides into a self-assembling system offers better antimicrobial activity. 17,21-24 To understand whether peptides formed nanoassembly inside nanocomposite, we have performed nanocomposite formation using different concentrations of peptides. Then, we have recorded a high-resolution SEM image. As shown in Figure S6A in the Supporting Information, we have not noted assembly formation for peptides when we used  $\alpha$ -defensin human neutrophil peptide-1 (6  $\mu$ g/mL), human  $\beta$ -defensin-1 (6  $\mu$ g/mL), and human cathelicidin LL-37 (6  $\mu$ g/mL)-attached nanocomposites. On the other hand, as shown in Figure S6B, we have noted small-assembly formation for peptides when we used  $\alpha$ -defensin human neutrophil peptide-1 (60  $\mu$ g/mL), human  $\beta$ -defensin-1 (60  $\mu$ g/mL), and human cathelicidin LL-37 (60 µg/mL)-attached nanocomposites. As shown in Figure S6C, huge-assembly formation for peptides is observed when we used  $\alpha$ -defensin human neutrophil peptide-1 (200  $\mu$ g/mL), human  $\beta$ -defensin-1 (200

 $\mu g/mL$ ), and human cathelicidin LL-37 (200  $\mu g/mL$ )-attached nanocomposite. We have also examined nanoassembly formation for peptides in solution phase using dynamic light scattering and SEM/TEM imaging. Our experimental observation indicates that assembly formation for peptides started when we used  $\alpha$ -defensin human neutrophil peptide-1 (55  $\mu g/mL$ ), human  $\beta$ -defensin-1 (55  $\mu g/mL$ ), and human cathelicidin LL-37 (55  $\mu g/mL$ )-attached nanocomposite.

### 3. CONCLUSIONS

We have developed novel antisuperbug nanocomposites via conjugation of naturally abundant biochar with human host  $\alpha$ defensin neutrophil peptide-1, human  $\beta$ -defensin-1, and cathelicidin LL-37 antimicrobial peptides. Current findings demonstrated that  $\alpha$ -defensin human neutrophil peptide-1, human  $\beta$ -defensin-1, and human cathelicidin LL-37-attached biochar-based nanocomposites can be used for capturing and removing broad-spectrum superbugs. The reported experimental data show that since the pore size of the nancomposite is much smaller than the size of superbugs, 100% of superbugs can be removed and captured from the environmental water sample via filtration. Remarkably, superbug-killing data show that HNP-1, HBD-1, and LL-37-attached nanocomposite can exhibit 100% killing efficiency for Gram-negative CRE E. coli and KPN superbugs as well as for Gram-positive MRSA and VRE superbugs. We found that the killing efficiency is >50% for Gram-positive and Gram-negative superbugs, when a mixture of HNP-1, HBD-1, and LL-37 peptides is used without nanocomposites. Our experimental observation indicates that capturing of superbugs by nanocomposites and imposing high membrane stress on bacteria surface are necessary for all three peptides to bind to the surface of bacteria and to obtain 100% killing efficiency. This study opens a new avenue for using bioinspired human host defense peptide-attached naturally abundant biochar-based nanocomposites against superbugs.

# ASSOCIATED CONTENT

# Supporting Information

The Supporting Information is available free of charge at https://pubs.acs.org/doi/10.1021/acsabm.0c00880.

Detailed synthesis; EDX mapping (Figure S1); FTIR spectra (Figure S2); XPS spectra (Figure S3); TEM images (Figures S4 and S5); SEM images (Figure S5); atomic composition from acid-modified biochar and nanocomposite (Table S1); and superbug-killing efficiency using biochar-based peptide-attached nanocomposite, peptide-attached nanoflakes, and peptide-attached gold nanoparticle (Table S2) (PDF)

# AUTHOR INFORMATION

## **Corresponding Author**

Paresh Chandra Ray — Department of Chemistry and Biochemistry, Jackson State University, Jackson, Mississippi 39217, United States; orcid.org/0000-0001-5398-9930; Email: paresh.c.ray@jsums.edu; Fax: +16019793674

# Authors

Ye Gao – Department of Chemistry and Biochemistry, Jackson State University, Jackson, Mississippi 39217, United States

- Avijit Pramanik Department of Chemistry and Biochemistry, Jackson State University, Jackson, Mississippi 39217, United States; oorcid.org/0000-0002-4623-2099
- Shamily Patibandla Department of Chemistry and Biochemistry, Jackson State University, Jackson, Mississippi 39217, United States
- Kaelin Gates Department of Chemistry and Biochemistry, Jackson State University, Jackson, Mississippi 39217, United States
- Glake Hill Department of Chemistry and Biochemistry, Jackson State University, Jackson, Mississippi 39217, United States
- Andrew Ignatius Department of Chemistry and Biochemistry, Jackson State University, Jackson, Mississippi 39217, United States

Complete contact information is available at: https://pubs.acs.org/10.1021/acsabm.0c00880

#### Note

The authors declare no competing financial interest.

#### ACKNOWLEDGMENTS

P.C.R. thanks NSF-PREM grant #DMR-1826886, NSF CREST grant #1547754, and NSF-RII-EPSCoR grant #1632899 for their generous funding.

#### REFERENCES

- (1) WHO. Antimicrobial Resistant Fact Sheet. http://www.who.int/mediacentre/factsheets/fs194/en/ (accessed May 6, 2020).
- (2) Theuretzbacher, U.; Bush, K.; Harbarth, S.; Paul, M.; Rex, J. H.; Tacconelli, E.; Thwaites, G. E. Critical analysis of antibacterial agents in clinical development. *Nat. Rev. Microbiol.* **2020**, *18*, 286–298.
- (3) Hernando-Amado, S.; Coque, T. M.; Baquero, F.; Martinez, J. L. Defining and combating antibiotic resistant from One Health and Global Health perspectives. *Nat. Microbiol.* **2019**, *4*, 1432–1442.
- (4) Årdal, C.; Balasegaram, M.; Laxminarayan, R.; McAdams, D.; Outterson, K.; Rex, J. H.; Sumpradit, N. Antibiotic development economic, regulatory and societal challenges. *Nat. Rev. Microbiol.* **2020**, *18*, 267–274.
- (5) Gray, D. A.; Wenzel, M. Multitarget approaches against multiresistant superbugs. ACS Infect. Dis. 2020, 6, 1346–1365.
- (6) Begum, S.; Davis, D.; Patibandla, S.; Gates, K.; Gao, Y.; Begum, S.; Ray, P. C. 2D and Heterostructure Nanomaterial Based Strategies for Combating Drug-Resistant Bacteria. *ACS Omega* **2020**, *5*, 3116–3130.
- (7) Gupta, A.; Mumtaz, S.; Li, C.-H.; Hussain, I.; Rotello, V. M. Combatting antibiotic-resistant bacteria using nanomaterials. *Chem. Soc. Rev.* **2019**, *48*, 415.
- (8) Dik, D. A.; Fisher, J. F.; Mobashery, S. Cell-Wall Recycling of the Gram-Negative Bacteria and the Nexus to Antibiotic Resistant. *Chem. Rev.* **2018**, *118*, 5952–5984.
- (9) El Meouche, I.; Dunlop, M. J. Heterogeneity in Efflux Pump Expression Predisposes Antibiotic-Resistant Cells to Mutation. *Science* **2018**, 362, 686–690.
- (10) Zong, Y.; Fang, F.; Meyer, K. J.; Wang, L.; Ni, Z.; Gao, H.; Lewis, K.; Zhang, J.; Rao, Y. Gram-scale total synthesis of teixobactin promoting binding mode study and discovery of more potent antibiotics. *Nat. Commun.* **2019**, *10*, No. 3268.
- (11) Xin, Q.; Shah, H.; Nawaz, A.; Xie, W.; Akram, M. Z.; Batool, A.; Tian, L.; Jan, S. U.; Boddula, R.; Guo, B.; Liu, Q.; Gong, J. R. Antibacterial Carbon-Based Nanomaterials. *Adv. Mater.* **2019**, *31*, No. 1804838.
- (12) Ray, P. C.; Khan, S. A.; Singh, A. K.; Senapati, D.; Fan, Z. Nanomaterials for Targeted Detection and Photothermal Killing of Bacteria. *Chem. Soc. Rev.* **2012**, *41*, 3193–3209.

- (13) Li, J.; Sexton, P. M. Targeting Antibiotic Resistant: From Diagnostics to Novel Antibiotics. *ACS Pharmacol. Transl. Sci.* **2020**, *3*, 371–372.
- (14) Dhesi, Z.; Enne, V. I.; O'Grady, J.; Gant, V.; Livermore, D. M. Rapid and Point-of-Care Testing in Respiratory Tract Infections: An Antibiotic Guardian? ACS Pharmacol. Transl. Sci. 2020, 3, 401–407.
- (15) Zhang, J.; Xu, J.; Ma, H.; Bai, H.; Lu, L.; Shu, C.; Li, H.; Wang, S.; Wang, C. Designing an Amino-Fullerene Derivative C70–(EDA)8 to Fight Superbacteria. ACS Appl. Mater. Interfaces 2019, 11, 14597–14607.
- (16) Hussain, S.; Li, F.; Qi, R.; Senthilkumar, T.; Zhao, H.; Chen, Y.; Liu, L.; Wang, S. Förster Resonance Energy Transfer Mediated Rapid and Synergistic Discrimination of Bacteria over Fungi Using a Cationic Conjugated Glycopolymer. ACS Appl. Bio Mater. 2020, 3, 20–28
- (17) Qi, R.; Zhang, N.; Zhao, H.; Liu, J.; Cui, J.; Xiang, J.; Han, Y.; Wang, S.; Wang, Y.; et al. Gemini Peptide Amphiphiles with Broad-Spectrum Antimicrobial Activity and Potent Antibiofilm Capacity. ACS Appl. Mater. Interfaces 2020, 12, 17220–17229.
- (18) Begum, S.; Pramanik, A.; Gates, K.; Gao, Y.; Ray, P. C. Antimicrobial Peptide-Conjugated MoS<sub>2</sub>-Based Nanoplatform for Multimodal Synergistic Inactivation of Bacteria. *ACS Appl. Bio Mater.* **2019**, *2*, 769–776.
- (19) Pramanik, A.; Gates, K.; Gao, Y.; Zhang, Q.; Han, F. X.; Rightshell, C.; Sardar, S.; Ray, P. C.; et al. Composites Composed of Polydopamine Nanoparticles, Graphene Oxide, and ε-Poly-L-lysine for Removal of Waterborne Contaminants and Eradication of Bacteria. ACS Appl. Nano Mater. 2019, 2, 3339–3347.
- (20) Sun, J.; Song, L.; Fan, Y.; Tian, L.; Luan, S.; Niu, S.; Ren, L.; Ming, M.; Zhao, J. Synergistic Photodynamic and Photothermal Antibacterial Nanocomposite Membrane Triggered by Single NIR Light Source. ACS Appl. Mater. Interfaces 2019, 11, 26581–26589.
- (21) Song, Y.; Lu, F.; Li, H.; Wang, H.; Zhang, M.; Liu, Y.; Kang, Z. Degradable Carbon Dots from Cigarette Smoking with Broad Spectrum Antimicrobial Activities against Drug-Resistant Bacteria. ACS Appl. Bio Mater. 2018, 1, 1871–1879.
- (22) Rigo, S.; Hürlimann, D.; Marot, L.; Malmsten, M.; Meier, W.; Palivan, C. G. Decorating Nanostructured Surfaces with Antimicrobial Peptides to Efficiently Fight Bacteria. *ACS Appl. Bio Mater.* **2020**, *3*, 1533–1543.
- (23) Vangara, A.; Pramanik, A.; Gao, Y.; Gates, K.; Begum, S.; Ray, P. C. Fluorescence Resonance Energy Transfer Based Highly Efficient Theranostic Nanoplatform for Two-Photon Bioimaging and Two-Photon Excited Photodynamic Therapy of Multiple Drug Resistant Bacteria. ACS Appl. Bio Mater. 2018, 1, 298–309.
- (24) Pramanik, A.; Jones, S.; Pedraza, F.; Vangara, A.; Sweet, C.; Williams, M. S.; Ruppa-Kasani, V.; Risher, S. E.; Sardar, D.; Ray, P. C. Fluorescent, Magnetic Multifunctional Carbon Dots for Selective Separation, Identification, and Eradication of Drug-Resistant Superbugs. ACS Omega 2017, 2, 554–562.
- (25) Jones, S.; Pramanik, A.; Kanchanapally, R.; Nellore, B. P. V.; Begum, S.; Sweet, C.; Ray, P. C. Multifunctional Three-Dimensional Chitosan/Gold Nanoparticle/Graphene Oxide Architecture for Separation, Label-Free SERS Identification of Pharmaceutical Contaminants, and Effective Killing of Superbugs. ACS Sustainable Chem. Eng. 2017, 5, 7175–7187.
- (26) Jones, S.; Sinha, S. S.; Pramanik, A.; Ray, P. C. Three-dimensional (3D) plasmonic hot spots for label-free sensing and effective photothermal killing of multiple drug resistant superbugs. *Nanoscale* **2016**, *8*, 18301–18308.
- (27) Viraka Nellore, B. P.; Kanchanapally, R.; Pedraza, F.; Sinha, S. S.; Pramanik, A.; Hamme, A. T.; Arslan, Z.; Sardar, D.; Ray, P. C. Bio-Conjugated CNT-Bridged 3D Porous Graphene Oxide Membrane for Highly Efficient Disinfection of Pathogenic Bacteria and Removal of Toxic Metals from Water. *ACS Appl. Mater. Interfaces* **2015**, 7, 19210–19218.
- (28) Pramanik, A.; Jones, S.; Gao, Y.; Sweet, C.; Begum, S.; Shukla, M. K.; Buchanan, J. P.; Moser, R. D.; Ray, P. C. A bio-conjugated chitosan wrapped CNT based 3D nanoporous architect re for

- separtion and inactivation of Rotavirus and Shigella waterborne pathogens. J. Mater. Chem. B 2017, 5, 9522-9531.
- (29) Liu, S.; Yuan, H.; Bai, H.; Zhang, P.; Lv, F.; Liu, L.; Dai, Z.; Bao, J.; Wang, S. Electrochemiluminescence for Electric-Driven Antibacterial Therapeutics. J. Am. Chem. Soc. 2018, 140, 2284–2291.
- (30) Dai, T.; Wang, C.; Wang, Y.; Xu, W.; Hu, J.; Cheng, Y. A Nanocomposite Hydrogel with Potent and Broad-Spectrum Anti-bacterial Activity. *ACS Appl. Mater. Interfaces* **2018**, *10*, 15163–15173.
- (31) Taheri-Ledari, R.; Maleki, A. Antimicrobial therapeutic enhancement of levofloxacin via conjugation to a cell-penetrating peptide: An efficient sonochemical catalytic process. *J. Pep. Sci* **2020**, 26, No. e3277.
- (32) Zhang, W.; Taheri-Ledari, R.; Hajizadeh, Z.; Zolfaghari, E.; Ahghari, R. M.; Maleki, A.; Hamblin, M. R.; Tian, Ye. Enhanced activity of vancomycin by encapsulation in hybrid magnetic nanoparticles conjugated to a cell-penetrating peptide. *Nanoscale* **2020**, *12*, 3855–3870.
- (33) Maleki, A.; Taheri-Ledari, R.; Rahimi, J.; Soroushnejad, M.; Hajizadeh, Z. Facile Peptide Bond Formation: Effective Interplay between Isothiazolone Rings and Silanol Groups at Silver/Iron Oxide Nanocomposite Surfaces. ACS Omega 2019, 4, 10629–10639.
- (34) Liu, W.-J.; Jiang, H.; Yu, H.-Q. Development of Biochar-Based Functional Materials: Toward a Sustainable Platform Carbon Material. *Chem. Rev.* **2015**, *115*, 12251–12285.
- (35) Xiao, X.; Chen, B.; Chen, Z.; Zhu, L.; Schnoor, J. L. Insight into Multiple and Multilevel Structures of Biochars and Their Potential Environmental Applications: A Critical Review. *Environ. Sci. Technol.* **2018**, *52*, 5027–5047.
- (36) Gao, Y.; Pramanik, A.; Begum, S.; Sweet, C.; Jones, S.; Alamgir, A.; Ray, P. C. Multifunctional Biochar for Highly Efficient Capture, Identification, and Removal of Toxic Metals and Superbugs from Water Samples. *ACS Omega* **2017**, *2*, 7730–7738.
- (37) Saquing, J. M.; Yu, Y.-H.; Chiu, P. C. Wood-Derived Black Carbon (Biochar) as a Microbial Electron Donor and Acceptor. *Environ. Sci. Technol. Lett.* **2016**, *3*, 62–66.
- (38) Shimabuku, K. K.; Paige, J. M.; Luna-Aguero, M.; Summers, R. S. Simplified Modeling of Organic Contaminant Adsorption by Activated Carbon and Biochar in the Presence of Dissolved Organic Matter and Other Competing Adsorbates. *Environ. Sci. Technol.* **2017**, *51*, 10031–10040.
- (39) Thompson, K. A.; Shimabuku, K. K.; Kearns, J. P.; Knappe, D. R. U.; Summers, R. S.; Cook, S. M. Environmental Comparison of Biochar and Activated Carbon for Tertiary Wastewater Treatment. *Environ. Sci. Technol.* **2016**, *50*, 11253–11262.
- (40) Gupta, S.; Bhatia, G.; Sharma, A.; Saxena, S. Host defense peptides: An insight into the antimicrobial world. *J. Oral Maxillofac. Pathol.* **2018**, 22, 239–244.
- (41) Hancock, R. E.; Haney, E. F.; Gill, E. E. The immunology of host defence peptides: Beyond antimicrobial activity. *Nat. Rev. Immunol.* **2016**, *16*, 321–334.
- (42) Lei, R.; Hou, J.; Chen, Q.; Yuan, W.; Cheng, B.; Sun, Y.; Jin, Y.; Ge, L.; Ben-Sasson, S. A.; Chen, J.; Wang, H.; Lu, W.; Fang, X. Self-Assembling Myristoylated Human  $\alpha$ -Defensin 5 as a Next-Generation Nanobiotics Potentiates Therapeutic Efficacy in Bacterial Infection. *ACS Nano* **2018**, *12*, 5284–5296.
- (43) Jung, S. W.; Lee, J.; Cho, A. E. Elucidating the Bacterial Membrane Disruption Mechanism of Human  $\alpha$ -Defensin 5: A Theoretical Study. *J. Phys. Chem. B* **2017**, *121*, 741–748.
- (44) Zhang, L. Disulfide Bonds Affect the Binding Sites of Human  $\beta$  Defensin Type 3 on Negatively Charged Lipid Membranes. *J. Phys. Chem. B* **2020**, 124, 2088–2100.
- (45) Lee, J.; Jung, S. W.; Cho, A. E. Molecular Insights into the Adsorption Mechanism of Human  $\beta$  Defensin -3 on Bacterial Membranes. *Langmuir* **2016**, 32, 1782–1790.
- (46) Shahmiri, M.; Enciso, M.; Adda, C. G.; Smith, B. J.; Perugini, M. A.; Mechler, A. Membrane Core-Specific Antimicrobial Action of Cathelicidin LL-37 peptide Switches Between Pore and Nanofibre Formation. *Sci. Rep.* **2016**, *6*, No. 38184.

- (47) Golla, R. M.; Mishra, B.; Dang, X.; Narayana, J. L.; Li, A.; Xu, L.; Wang, G. Resistome of Staphylococcus aureus in Response to Human Cathelicidin LL-37 and Its Engineered Antimicrobial Peptide. *ACS Infect. Dis.* **2020**, *6*, 1866–1881.
- (48) Mishra, B.; Golla, R. M.; Lau, K.; Lushnikova, T.; Wang, G. Anti-staphylococcal biofilm effects of human cathelicidin peptides. *ACS Med. Chem. Lett.* **2016**, *7*, 117–121.